



# Pyrrole-based enone dyes as radical photoinitiator under 405/460 nm LED lamp: The effect of ketone structure

Tanlong Xue<sup>1</sup>, Yang Li<sup>1</sup>, Liqun Tang, Ruifen Tang, Jun Nie, Xiaoqun Zhu<sup>\*</sup>

State Key Laboratory of Chemical Resource Engineering, Beijing Laboratory of Biomedical Materials, College of Materials Science and Engineering, Beijing University of Chemical Technology, Beijing, 100029, PR China

## ARTICLE INFO

### Keywords:

Pyrrole-based dyes  
Photopolymerization  
Ketone structure  
Double bond rotation  
Internal conversion

## ABSTRACT

Enone dyes have gained tremendous attention as photoinitiator in visible light induced photopolymerization. However, the structure-relationship of the enone's photochemical-reactivity, which strongly determined their initiation efficiency, were not fully uncovered. In this work, pyrrole-based enones (PYOs) were synthesized by the condensation of N-methylpyrrole-2-aldehyde and four different ketones, yielding C3PY, C6PY, C6NPY, and C6SPY. It was found that variation of ketone part slightly affected their absorption properties but significantly changed their photophysical behavior. Accordingly, initiation performance of PYOs toward an acrylate monomer, when co-used with onimum salt or triethanolamine as additives, differentiated with each other, which is in line with the photolysis experiment results. DFT calculation proved that imposing a six-member ring on ketone part decreases the molecular planarity of C6PY, C6NPY, and C6SPY, which in turn, enhances their internal conversion yield and decrease their photochemical reactivity. This work provides meaningful information for the structure-property relationships territory of enone dyes.

## 1. Introduction

Due to the temporally and spatially controllable manners, photopolymerization technology has been applied to various filed including sophisticated industrial filed and cutting-edge academic area [1,2]. Among of the photopolymerization, photoinitiator absorbs proper light and subsequently generates active species (radical or cation). Due to the latent harm of mercury lamp to living body and environment, current interest is to use light emitting diode (LED) as visible light irradiance [3–6].

In the last decade, great effort has been dedicated to the development of photo initiating system under soft light, many kinds of synthesized dyes were investigated. However, some of the reported dyes were often suffered from tedious synthetic procedure, which enabled some limitation for the practical application [7–17]. Enone dyes can be facily synthesized by aldol condensation and have been reported as two-photo photoinitiator, some of them possess both large two-photon cross section and good initiation ability [18–23]. In recent years, the enone dyes got renaissances as one-photon initiator. Wang's group reported aromatic amines based enone dyes, when the triethanolamine or ONI was used as co-initiator, they can initiate the acrylate and ceramic suspension of

acrylate monomer under blue/green light [24,25]. Nie's group reported furans and pyrrole-based enone dye and evaluate their initiation performance under UV-LED lamp [26–28]. Lalevée and Xiao group investigated several kinds of ketone dyes with different ketone structure and peripheral group and applied these dyes as photoinitiator in 3D and 4D printing systems [29–33].

Up to now, many enone dyes bearing different periphery group and ketone parts have been reported [30,34]. However, the effect of different ketone structures was rarely systematically studied and summarized. To explore the influence of ketone part on the photochemical reactivity of enone dyes, the periphery group must be consistent to preclude others factor. In our previous work, pyrrole group was found to be a promising phenyl-free group for its electron-rich nature and hydrogen donor ability [27].

In this work, pyrrole-based enones (PYOs) were synthesized by one-spot condensation of N-methylpyrrole-2-aldehyde and acetone, cyclohexanone, tetrahydrothiopyran-4-one, and 1-Methyl-4-piperidone, respectively. Cyclobutanone and cyclopentanone were not of our interests because of their rigid structure, which would decrease the solubility of target molecules. The as synthesized PYOs were well characterized by NMR, FT-IR, HRMS spectroscopy. The photophysical

\* Corresponding author.

E-mail address: [zhuxq@mail.buct.edu.cn](mailto:zhuxq@mail.buct.edu.cn) (X. Zhu).

<sup>1</sup> These authors contributed equally to this work.

properties were investigated by UV–Vis and Fluorescence spectrometer. The photochemical behavior of PYOs themselves and PYOs/co-initiators in solution under a 405 nm LED irradiation were investigated by steady state photolysis experiment. The initiation performance of PYOs to an acrylate monomer, when combined with TEOA or ONI, were evaluated by Real-Time FT-IR spectroscopy. To get insight into PYOs, quantum calculations were performed. These systematic investigation to PYOs will greatly be beneficial to the further blossom of enone dyes photoinitiator.

## 2. Experimental details

### 2.1. Materials and general instruments

All reagents and solvents used are reagent grade, which were obtained from commercial sources and used without further purification. Acetonitrile, ethanol, acetone, and sodium hydroxide were purchased from Beijing Chemical Works (Beijing, China). Triethanolamine (TEOA) was used as a reference tertiary amine and Iodonium bis(4-methylphenyl) hexafluorophosphate (ONI) was used as a reference iodonium salt. Tripropylene glycol diacrylate (TPGDA), purchased from Guangzhou Lihou Trading Co. Ltd, China) was chosen as the monomers for free radical photopolymerization. N-Methylpyrrole-2-carboxaldehyde, cyclohexanone, tetrahydrothiopyran-4-one, and 1-Methyl-4-piperidone was purchased from Innochem (Beijing, China). [Scheme 1](#) summarizes the abbreviations and structures of selected compounds in this study.

$^1\text{H}$  NMR and  $^{13}\text{C}$  NMR spectra were recorded on a Bruker AV NMR spectrometer. FT-IR spectra were recorded on a Nicolet 5700 instrument (Thermo Electron corporation, Waltham, MA). MS measurements were carried out on an ESI-MS spectrometer (Xevo G2 Qtof, Waters). Melting point was obtained with a differential thermal scanning calorimeter (METTLER TOLEDO). LED irradiation source were purchased from SHENZHEN LAMPLIC TECH CO., LTD. The light intensity was measured by using an ultraviolet–visible radiometer which was fabricated by Beijing Normal University, China.

### 2.2. Synthesis of PYOs

The synthetic route for PYOs is shown in [Scheme 2](#). The corresponding  $^1\text{H}$  NMR,  $^{13}\text{C}$  NMR, FT-IR, HRMS spectra, and DSC curve are presented in [Fig. S1–S17](#).

#### 2.2.1. (1E,4E)-1,5-bis(1-methyl-1H-pyrrol-2-yl) penta-1,4-dien-3-one (C3PY)

N-Methylpyrrole-2-carboxaldehyde (10 mmol, 1.09 g) and acetone (5 mmol, 0.29g) was dissolved in 30 ml ethanol, the mixture was heated to reflux under string. Then, the sodium hydroxide aqueous solution (1.0 g NaOH/10 mL H<sub>2</sub>O) was added dropwise to the reaction system. After N-Methylpyrrole-2-carboxaldehyde was almost consumed, the reaction was cooled down to room temperature, during which yellow participation appeared. The crude product obtained by filtered was further recrystallized in ethanol to give a yellow crystal. Yield: 75%. Mp: ca. 150 °C.  $^1\text{H}$  NMR (400 MHz, CD<sub>3</sub>CN)  $\delta$  7.65 (d,  $J$  = 15.6 Hz, 2H), 6.90 (d,  $J$  = 2.0 Hz, 2H), 6.87 (d,  $J$  = 15.6 Hz, 2H), 6.83–6.79 (m, 2H),

6.22–6.16 (m, 2H), 3.77 (s, 6H).  $^{13}\text{C}$  NMR (101 MHz, CD<sub>3</sub>CN)  $\delta$  187.15, 129.66, 129.33, 127.45, 120.80, 111.59, 108.88, 33.49. FT-IR (KBr):  $\text{cm}^{-1}$  3119, 3097, 1652, 1610, 1558, 1383. HRMS (ESI-TOF)  $m/z$ : [M + H]<sup>+</sup> Calcd for C<sub>15</sub>H<sub>16</sub>N<sub>2</sub>O<sub>2</sub>H 241.1263; found: 241.1286.

#### 2.2.2. 2,6-bis((1-methyl-1H-pyrrol-2-yl)methylene)cyclohexan-1-one (C6PY)

The synthesis of C6PY is similar with the C3PY. Yellow crystal. Yield: 70%. Mp: ca. 176 °C.  $^1\text{H}$  NMR (400 MHz, DMSO)  $\delta$  7.63 (s, 2H), 7.07 (d,  $J$  = 1.7 Hz, 2H), 6.54 (d,  $J$  = 3.1 Hz, 2H), 6.20 (dd,  $J$  = 3.5, 3.0 Hz, 2H), 3.71 (s, 6H), 2.76 (t,  $J$  = 5.5 Hz, 4H), 1.83–1.73 (m, 2H).  $^{13}\text{C}$  NMR (151 MHz, DMSO)  $\delta$  186.81, 130.48, 129.04, 127.09, 122.98, 114.28, 108.96, 33.85, 27.93, 21.73. FT-IR (KBr):  $\text{cm}^{-1}$  3123, 3103, 2935, 1645, 1591, 1546, 1380. HRMS (ESI-TOF)  $m/z$ : [M + H]<sup>+</sup> Calcd for C<sub>18</sub>H<sub>20</sub>N<sub>2</sub>O<sub>2</sub>H 281.1576; found: 281.1668.

#### 2.2.3. 1-Methyl-3,5-bis((1-methyl-1H-pyrrol-2-yl)methylene)piperidin-4-one (C6NPY)

The synthesis of C6NPY is similar with the C3PY. Brown crystal. Yield: 69%. Mp: ca. 122 °C.  $^1\text{H}$  NMR (400 MHz, DMSO)  $\delta$  7.55 (s, 2H), 7.12–7.08 (m, 2H), 6.42 (dd,  $J$  = 3.9, 1.0 Hz, 2H), 6.22 (dd,  $J$  = 3.5, 2.8 Hz, 2H), 3.72 (s, 6H), 3.59 (s, 4H), 2.45 (s, 3H).  $^{13}\text{C}$  NMR (151 MHz, DMSO)  $\delta$  184.47, 128.28, 128.07, 127.61, 121.35, 114.83, 109.25, 56.58, 45.54, 33.86. FT-IR (KBr):  $\text{cm}^{-1}$  3103, 2937, 2764, 1657, 1597, 1561, 1383. HRMS (ESI-TOF)  $m/z$ : [M + H]<sup>+</sup> Calcd for C<sub>18</sub>H<sub>21</sub>N<sub>3</sub>O<sub>2</sub>H 296.1685; found: 296.1767.

#### 2.2.4. 3,5-bis((1-methyl-1H-pyrrol-2-yl)methylene)tetrahydro-4H-thiopyran-4-one (C6SPY)

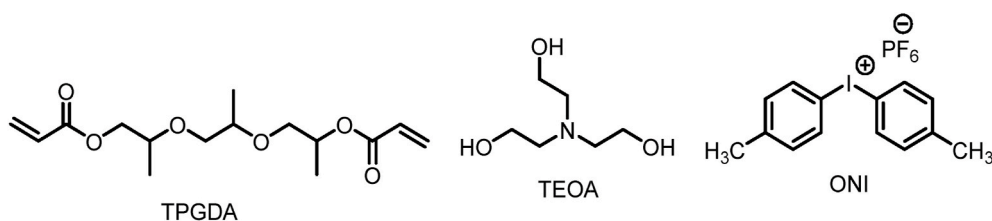
The synthesis of C6SPY is similar with the C3PY. Yellow crystal. Yield: 71%. Mp: ca. 133 °C.  $^1\text{H}$  NMR (400 MHz, DMSO)  $\delta$  7.61 (s, 2H), 7.10 (dd,  $J$  = 2.2, 1.7 Hz, 2H), 6.59 (dd,  $J$  = 4.0, 1.1 Hz, 2H), 6.21 (dd,  $J$  = 3.5, 2.7 Hz, 2H), 3.89 (s, 4H), 3.71 (s, 6H).  $^{13}\text{C}$  NMR (151 MHz, DMSO)  $\delta$  185.85, 128.20, 128.10, 127.56, 122.88, 114.73, 109.18, 33.91, 29.24. FT-IR (KBr):  $\text{cm}^{-1}$  3102, 2920, 1646, 1586, 1548, 1376. HRMS (ESI-TOF)  $m/z$ : [M + H]<sup>+</sup> Calcd for C<sub>17</sub>H<sub>18</sub>N<sub>2</sub>O<sub>2</sub>S 299.1140; found: 299.1227.

### 2.3. Computational procedure

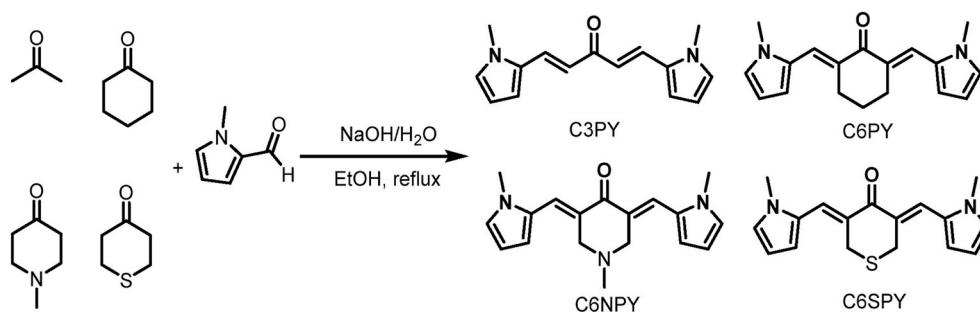
All the density functional theory (DFT) and time-dependent density functional theory (TDDFT) calculations were completed within Gaussian 09 program package [44]. Gaussian View 5.0 was used to visualize and analyze the calculation results. B3LYP/6-31G (d, p) was adopted to ground state (S<sub>0</sub>) geometry optimization and frequency analysis. Based on the optimized S<sub>0</sub> geometry, the vertical singlet transitions were calculated at (TDDFT) B3LYP/6-31G (d, p) level with SMD as solvent model. According to our experiment, acetonitrile was chosen as solvent. The potential energy surface of S<sub>0</sub> and T<sub>1</sub> were constructed at (U)B3LYP 6-31G (d, p) level to compare their relative energy. Coordinates of molecular structures were provided in supporting information.

### 2.4. Photopolymerization experiment

The free radical photopolymerizations were carried out under



**Scheme 1.** Abbreviations and structures of some compounds employed in this study.



Scheme 2. Synthetic route for PYOs.

laminated condition. The photosensitive formulations were photocured in 1 mm thick silicone molds with a 10 mm diameter center. The formulation was irradiated by 405/460 nm LED lamp. The infrared spectra of uncured resin were collected by Real-Time Fourier transform infrared spectrometer (Nicolet 5700, 7000–4000  $\text{cm}^{-1}$  wavenumber range). The double bond conversion (DBC) profiles were calculated from the decay of the characteristic peak at 6157  $\text{cm}^{-1}$  by using the following equation [35]:

$$\text{Double bond conversion\%} = [1 - (S_t / S_0)] \times 100\%$$

where  $S_t$  is the area of absorbance peak at  $t$  time and  $S_0$  is the initial area before irradiation.

## 2.5. UV-vis absorption and photolysis experiment

The UV-vis spectra were recorded by using a UV-5200 (UNICO) UV-vis spectrophotometer. The steady state photolysis was performed under 405 nm LED lamp, the incident light intensity at the cuvette surface was set to 80  $\text{mW}/\text{cm}^2$ . The solutions were previously  $\text{N}_2$  bubbled 10 min to eliminate the influence of oxygen. Continuous magnetic stirring was provided during the photolysis. After the given irradiation time, the absorption spectrum was obtained.

## 2.6. Fluorescence emission properties

### 2.6.1. Emission wavelength and quantum yield

The fluorescence emission wavelength studied using an F-4500 (Hitachi High-Technologies Corporation) fluorescence spectrophotometer. The relative emission quantum yield was calculated by using quinine sulfate dihydrate (SK) in 0.1 M sulfuric acid aqueous solution as reference ( $\Phi_R = 0.54$ ). The relative emission quantum yield of between PYOs were normalized by using C3PY as a standard ( $\Phi_f = 1$ ).

### 2.6.2. Time correlated single photon counting

The excited state lifetimes were obtained by using a full-function steady-state transient fluorescence spectrometer (FLS980, Edinburgh Instruments). The apparatus uses a Nano LED (390 nm) generating pulses of about 100–10 ps for the excitation. The fluorescence intensity decay profiles were recorded in acetonitrile in a quartz cell. A silica colloidal solution LUDOX® was used to evaluate the impulse response function (IR) of the apparatus.

## 3. Results and discussion

### 3.1. Synthesis

All PYOs could be synthesized through one-step classical aldol condensation reaction between N-Methylpyrrole-2-carboxaldehyde and corresponding ketones. After recrystallization, PYOs with acceptable purity were obtained, the yield is of being 69%–75%. The high coupling constant (15.6 Hz) indicates that the structure of C3PY a pure E, E

configuration. While for C6PY, C6NPY, and C6SPY, the absolute structure configuration cannot be accurately identified due to the lack of a coupling constant. However, the characteristic peaks for the Z-isomers appear at  $\sim 6.8$  ppm. Since PYOs's proton signal in double bond appeared at 7.55–7.63 ppm, it is highly suggested that PYOs are pure E, E isomer [19].

### 3.2. UV-vis absorption and fluorescence emission properties

As can be seen in Fig. 1(a) and Table 1, PYOs displayed strong absorption bands around 410–420 nm, their maximum absorption wavelengths are similar, indicating that the six-member ring on the ketone part has little effect on the absorption ability. The molar extinction efficiency of PYOs at their maximum absorption wavelength follows the order: C6NPY > C6PY > C3PY > C6SPY. Fig. 2 demonstrated that PYOs displayed very similar HOMO-LUMO gap and transition characters, which is in line with their alike absorption properties. The electron densities in PYOs have same tendency that transferred from the whole molecular to the central ketone part during HOMO-LUMO transition. Therefore, the observed absorption band could be ascribed to the  $\pi \rightarrow \pi^*$  transition bearing intermolecular charge transfer feature. Moreover, in C6PY, C6NPY and C6SPY, there are few electron densities in six-member ring contributed to the HOMO-LUMO transition, which may lead to their slightly different absorption intensity.

In line with the absorption spectrum, the fluorescence emission wavelength of PYOs is almost identical (see normalized fluorescence spectrum, Figure. S18). However, their fluorescence emission intensity, varied a lot. Fig. 1 (b) shows that under their optimum excitation wavelength and same instrument parameters, C3PY has the strongest emission band located at 499 nm, while others of PYOs exhibited very weak band. Efforts made to calculate the emission yield indicated that the quantum yield of C3PY in acetonitrile is lower to 0.014% (Figure. S19). While for others of PYOs, no acceptable emission spectra could be obtained under same instrumental parameters. Since C3PY has highest quantum yield among PYOs, the yield of C6PY, C6NPY, and C6SPY were normalized by using C3PY as standard ( $\Phi_f = 1$ ). By comparing their integrated emission area (Fig. 1(b)), their yield relative to C3PY are collected in Table 2. The fluorescence quantum yield of C3PY are around ten folds higher than that PYOs bearing six-member ring. The average fluorescence lifetime of C3PY is 0.12 ns, this very short lifetime is very closed to the instrument response time. For others of PYOs, the lifetime is five to ten times longer than C3PY (Figure. S20).

### 3.3. Steady state photolysis

During photopolymerization induced by bimolecular initiation system, the photoinitiator react with additive through direct hydrogen- abstraction or redox mechanism, which would lead the consumption of photoinitiator. Therefore, steady state photolysis experiment was conducted to investigate the photochemical reaction of photoinitiator itself and photochemical reaction between photoinitiator and additives.

As shown in Fig. 3(a, b, c, and d), the photolysis of individual PYOs is

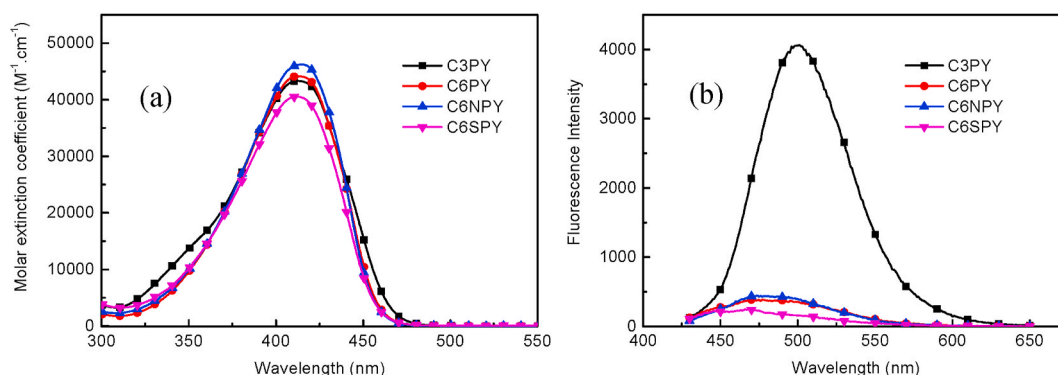


**Fig. 1.** (a) Absorption [PYOs] =  $2.0 \times 10^{-5}$  M and (b) fluorescence spectra [PYOs] =  $2.0 \times 10^{-6}$  M of PYOs in acetonitrile. The fluorescence spectra were obtained at their maximum excitation wavelength, excitation condition: EX: split 10 nm, EM split 10 nm. Voltage 700 V.

**Table 1**

The photophysical property of PYOs in acetonitrile.

	$\lambda_{\max}^a$ (nm)	$\epsilon_{\max}^b$ ( $M^{-1} \text{cm}^{-1}$ )	$\epsilon_{405}^c$ ( $M^{-1} \text{cm}^{-1}$ )	$\epsilon_{460}^c$ ( $M^{-1} \text{cm}^{-1}$ )	$\lambda_{\text{em}}^d$ (nm)	$\Phi_f^e$	$\tau_{\text{av}}^f$ (ns)
C3PY	414	43300	42200	6400	499	1.0	0.12
C6PY	413	44100	42800	3100	498	0.12	0.62
C6NPY	415	46200	44500	2650	495	0.11	0.51
C6SPY	412	40400	39590	2660	497	0.07	1.17

<sup>a</sup> Maximum absorption wavelength of PYOs. <sup>b, c</sup> Molar extinction coefficient at maximum wavelength, 405 nm, and 460 nm. <sup>d</sup> Emission wavelength of PYOs. <sup>e</sup> Normalized fluorescence quantum yield between PYOs by using C3PY as standard, <sup>f</sup> average fluorescence lifetime of PYOs.

very different. The absorption band of C3PY declined continuously and rapidly after given irradiation time. According to our previous study, this very fast photobleaching may result from the electron/proton transfer reaction (Scheme S1 eq(a)) between an excited C3PY and a ground C3PY. However, for C6PY, C6NPY and C6SPY, the fast absorbance reduction occurred after 2 s light irradiation, and an isosbestic point appeared simultaneously. Very similar photochemical behaviors were also observed previously for 2,6-bis(furan-2-ylmethylidene) cyclohexan-1-one (BFC), which also bearing a cycloheptanone, and these kinds of spectral transformation were ascribed to the isomerization [36]. Therefore, it is deduced that double bond rotation occurred in C6PY, C6NPY and C6SPY, resulting corresponding Z-Z or Z-E isomers, which cannot be clearly identified at this stage (Scheme S1 eq(b)). The theoretical relative energies, electronic geometries, FMOs and first

excited energies of possible isomer could be seen in Table S1-S2). Moreover, these isomers cannot go back to their initial state after being placed in dark for 24 h (data not shown). What obviously different with the reported sustaining photobleaching of BFC isomer is that, the photostability of the generated isomer in our work is relative stable. Subsequent irradiation until 60 s, the absorbance band of PYOs only decreased slightly, among which C6SPY is the most stable one. Therefore, it seems that the peripheral group also have very significant influence on the photochemical reactivity of enone dyes. The above consequence indicates that the ketone part of C3PY has the highest photochemical reactivity, on which electron/proton transfer could happen, while imposing a six-member ring decreased the photochemical of ketone in C6PY, C6NPY and C6SPY, which was evidenced by their stable behavior under light irradiation.

Fig. 3(e, f, g, h) shows that the addition of a common-used hydrogen donor, TEOA, has little effect on the photolysis rate of PYOs, indicating

**Table 2**

The assessed photophysical process parameters for PYOs.

PYOs	$K_f^a$ ( $10^9 \text{ s}^{-1}$ )	$K_{\text{IC}}^b$ ( $10^9 \text{ s}^{-1}$ )	$K_{\text{IC}}/K_f$
C3PY	8.33	0	0
C6PY	0.19	1.42	7.33
C6NPY	0.22	1.75	8.09
C6SPY	0.06	0.79	13.29

<sup>a</sup> Fluorescence emission rate,  $K_f = 1/\tau_{\text{av}} \times \Phi_f$ .

<sup>b</sup> Internal conversion rate,  $K_{\text{IC}} = 1/\tau_{\text{av}} \times \Phi_{\text{IC}}$ ,  $\Phi_{\text{IC}} = 1 - \Phi_f$  (with the assumption that the  $\Phi_{\text{ISC}}$  of PYOs are at same level).

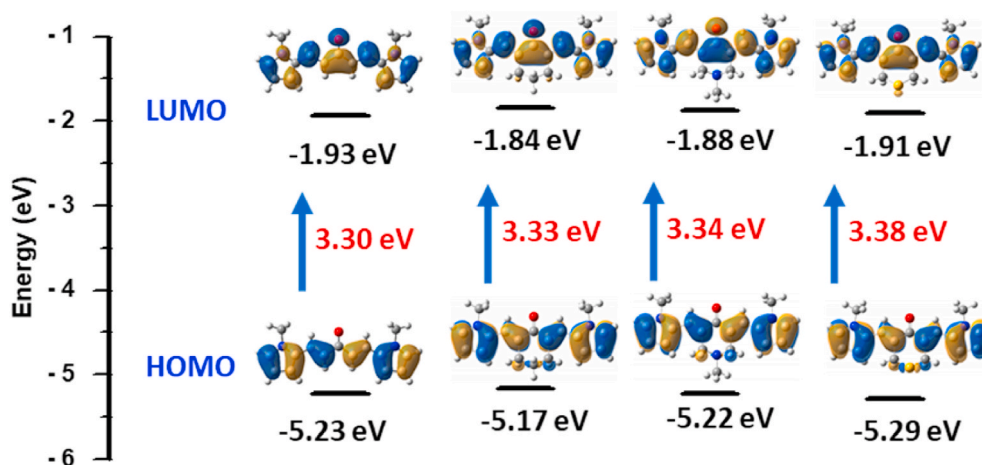


**Fig. 2.** Frontiers molecular of PYOs calculated at B3LYP/6-31G (d, p) level. HOMO: Highest occupied molecular orbitals; LUMO: Lowest unoccupied molecular orbitals.

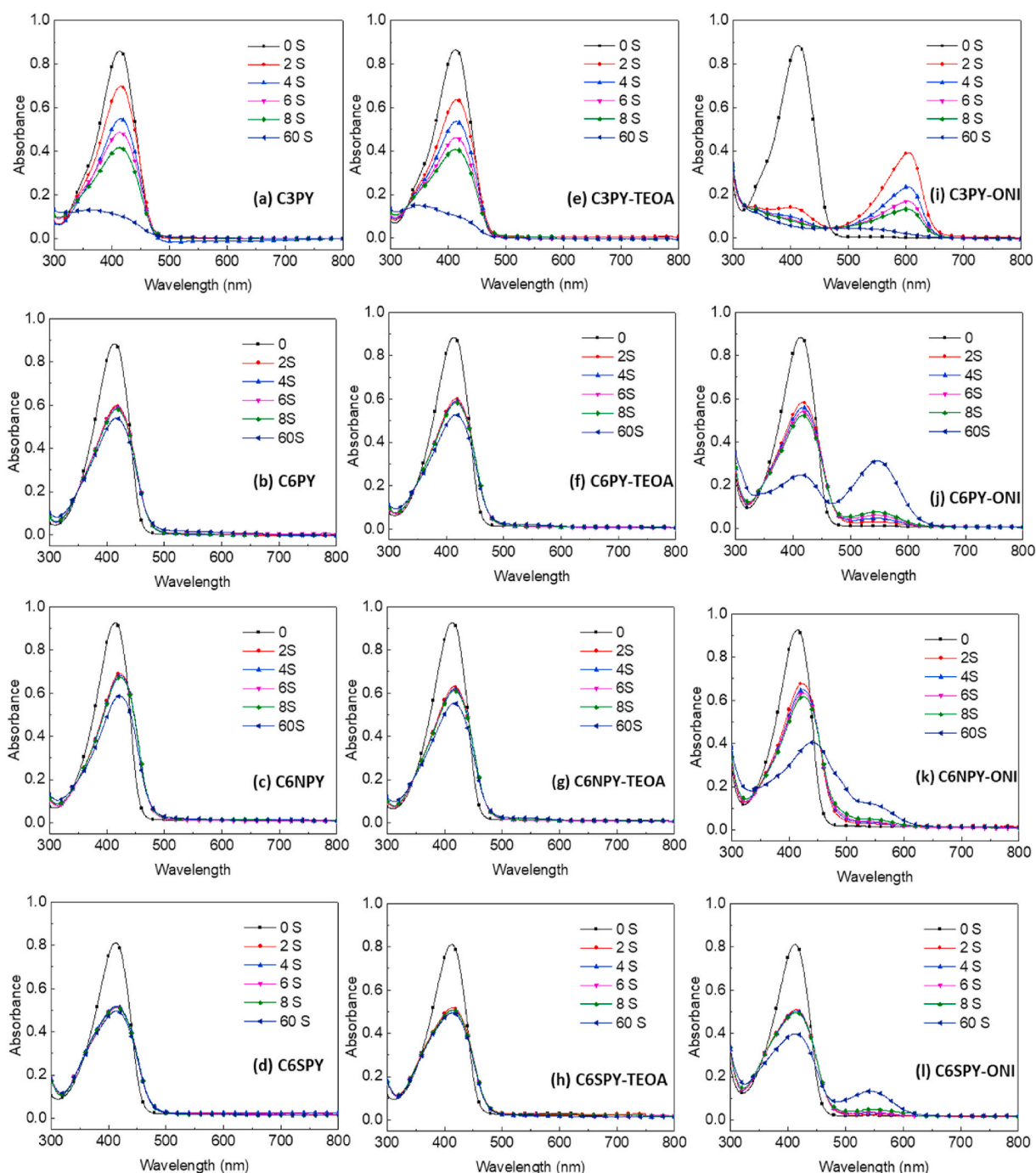


**Fig. 3.** The absorption spectra of (a–d) PYOs along, (e–h) PYOs/TEOA, and (i–l) PYOs/ONI in acetonitrile under 405 nm LED Lamp irradiation. [PYOs] =  $2.0 \times 10^{-5}$  M, [TEOA] =  $6.0 \times 10^{-4}$  M, [ONI] =  $4.0 \times 10^{-4}$  M.

that the interaction of TEOA and PYOs is not strong (Scheme S1 eq(c)). The reaction between PYOs and ONI (Scheme S1 eq(d)) is obviously faster than PYOs/TEOA (Fig. 3(i, j, k, and l)). Among them, the C3PY displayed the highest reactivity toward ONI. Only 2 s irradiation time led to the almost total consumption of C3PY (Fig. 3(i)). While for C6PY, C6NPY, and C6SPY, their absorption spectra transformation with the addition of ONI are almost as same as their corresponding one-component photolysis after the first 2 s irradiation. Hence, it could be concluded that, as to C6PY, C6NPY, and C6SPY, their isomerization rate is very fast and their reactions on ONI happened at their corresponding isomer. Aside from the decline of main absorption band, a new absorption band appeared at 500 nm–600 nm during the photolysis of

PYOs and ONI. This phenomenon could be ascribed to the interaction between PYOs and protonic acid released in PYOs/ONI system, since ONI is a well-known acid generator [37,38].

### 3.4. Photopolymerization kinetics

Fig. 4 provides the polymerization profiles of TPGDA versus irradiation time by using PYOs and PYOs/additive bimolecular as initiation system. C3PY could slowly initiate the polymerization of TPGDA, the DBC is around 65% after 600 s irradiation, while at same time scale, the DBC are 14%, 6%, and 3% for C6NPY, C6PY, and C6SPY, respectively (Fig. 4(a)). These profiles indicated that only C3PY could efficiently

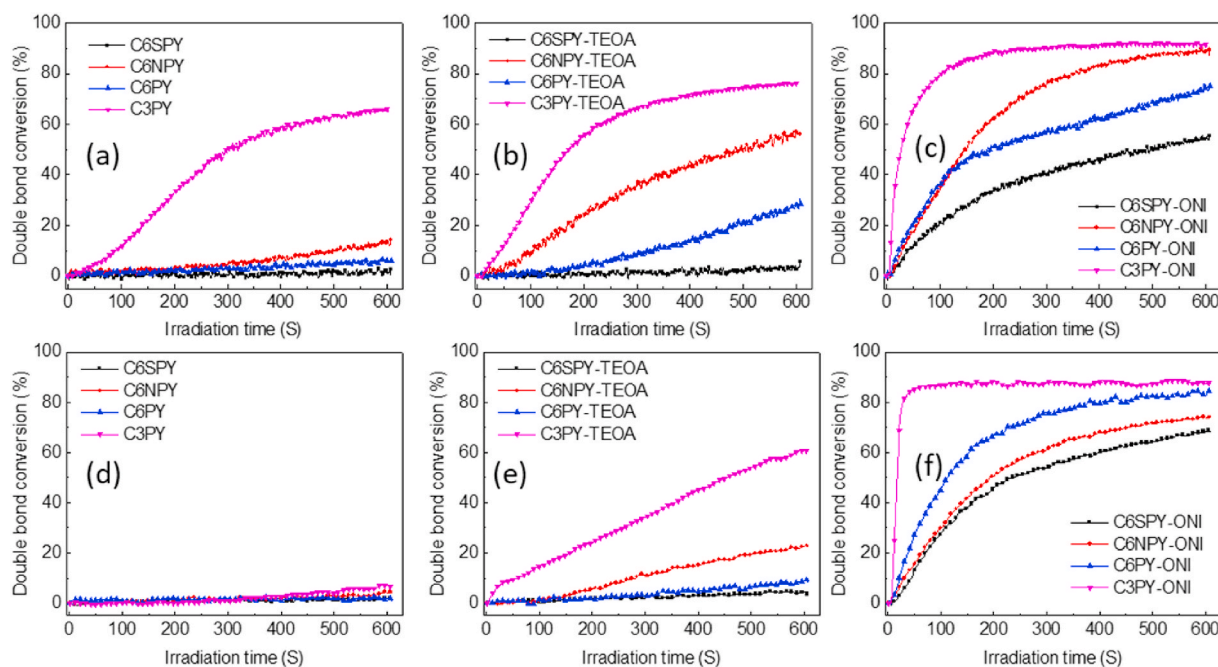


**Fig. 4.** Polymerization profiles of TPGDA by using PYOs, PYOs/TEOA, PYOs/ONI as initiation system (a, b, and c: Under 405 nm LED; d, e, f: Under 460 nm). C3PY: 0.1% wt, TEOA: 3%, ONI: 2%, weight fraction relative to TPGDA, the light intensity was set to around 130 mw/cm<sup>2</sup>.

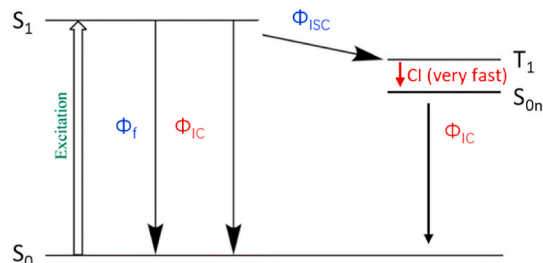
generate radical, which is in line with its rapid and continuous photobleaching behavior during photolysis experiment. By the addition of TEOA the polymerization rate and final DBC were improved at different extent although the addition of TEOA has neglectable acceleration on the photolysis rate of PYOs (Fig. 4(b)). The DBC at 200 s of C3PY/TEOA is 56% while it is 33% for C3PY after same irradiation time. Fig. 4(c) illustrated that PYOs/ONI exhibited the best initiation efficiency. After 600 s irradiation, the DBC are 92%, 89%, 75%, and 55% for C3PY, C6NPY, C6PY, and C6SPY, respectively.

Under 460 nm, PYOs displayed weak initiation efficiency (Fig. 4(d)) probably due to their weak absorption ability under this wavelength. Among PYOs/TEOA system (Fig. 4(e)), C3PY exhibited acceptable polymerization rate, the final DBC is 60% while others of PYOs are lower to 20%. As to PYOs/ONI system (Figure. (f)), all of them can efficiently trigger the polymerization. The overall trend is C3PY > C6PY > C6NPY > C6SPY. This trend is at some extent different with that of under 405 nm, which may due to the counterbalance of light penetration ability and photochemical reactivity. In short, C3PY has the best initiation performance among PYOs either in their one-component or bi-molecular systems. The polymerization ability of PYOs/ONI system is obviously higher than that of PYOs/TEOA, which is in line with the photolysis experiments.

### 3.5. Analysis of photophysical process

#### 3.5.1. Excited singlet states

Such big different photochemical reactivity between PYOs drives us to investigate their photophysical process of PYOs because photophysical process is competitive with the photochemical process. As shown in Scheme 3, after being excited to singlet state, PYOs could undergo intersystem crossing (ISC) to triplet states, internal conversion (IC) to ground states, and fluorescence emission (f), these photophysical processes are competitive [39]. The ISC generally need sufficient spin-orbital coupling, thus the ISC yield of PYOs would not expect to vary a lot. Table 2 proved that, for C6PY, C6NPY, and C6SPY, the  $K_{IC}$  is 7–13 times higher than the  $K_f$ , which demonstrated most of singlet excited state molecules were deactivated through IC. The largest  $K_{IC}/K_f$  of C6SPY indicates that C6SPY tends to lost its excited energy through IC



**Scheme 3.** The photophysical process of PYOs after being excited.

at the highest extent among PYOs, therefore resulting in C6SPY's lowest photoinitiation ability. Moreover, the  $K_{IC}$  is assessed at the order of  $10^9$  s<sup>-1</sup>. What must be noted is that, the  $K_{IC}$  reported here is at some extent underestimated, because the emission quantum yield of PYOs used in Table 2 are obviously higher than their actual value. For brief summary, the excited C6PY, C6NPY, and C6SPY tend to dissipate their excited energy through IC, and the  $K_{IC}$  is very fast, of which the photochemical reaction may hardly compete with. Those results could well explain their low photo-reactivity comparing with C3PY though they have relative longer fluorescence lifetime (Table 1).

Since carbon-carbon double bond rotation is a domain IC channel to deactivate excited states, it is postulated that the existence of six-member ring on ketone significantly enhance the double bond rotation [40]. To examine our assumption, the optimized electronic geometries of PYOs were analysed. As given in Fig. 5, C3PY presents the best planarity, the dihedral around double bond is almost 180°. As to C6PY, the dihedral around double is around 177°, which indicates that the existence of six-member ring decreased the planarity. Moreover, as pointed by black arrow, the bond length between two hydrogen, B (9, 23), in C3PY is 2.53 Å. While for C6PY, one of the hydrogens in six-member ring is likely to repel with the hydrogen in pyrrole ring as evidenced by their relative short bond length B (37, 13) 2.17 Å. Similar structural characters were also found in C6NPY and C6SPY (See Figure. S21). Therefore, it is established the six-member ring has considerable repulsive effect on the peripheral pyrrole group, which may accelerate

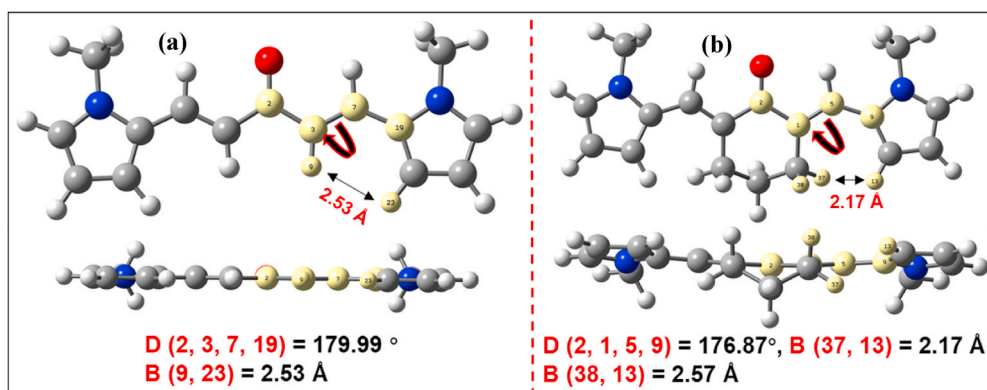


Fig. 5. The ground state geometries of (a) C3PY and (b) C6PY optimized at B3LYP/6-31G (d, p) level.

the rotation of double bond.

Fluorescence quenching is an important method to examine the electron transfer quantum yields ( $\phi_{et}$ ) between photoinitiator/sensitizer and co-initiator, reflecting the photochemical reaction occurred in singlet excited state [15,28,41]. In our case, fluorescence quenching of PYOs were performed with TEOA or ONI as quencher. However, no reliable data could be obtained for the  $\phi_{et}$  calculation (data not shown). It must be noted PYOs are almost nonfluorescent, the fluorescence quantum of C3PY is 0.014% (Figures S19), while much lower fluorescence quantum yields are expected for others of PYOs, so the photochemical reaction between PYO and TEOA or ONI is unlikely to occur in the singlet excited state. Therefore, the fluorescence quenching may inapplicable if the tested molecules are almost nonfluorescent.

### 3.5.2. Excited triplet states

The very fast excited state deactivation could occur if the potential energy surface (PES) of excited state and ground state is highly closed or even crossed [40,42,43]. This phenomenon was defined as conical intersection (CI) (Scheme 3). Since the triplet states have lower energy than singlet state, in the case of PYOs, the lowest triplet state and ground states PES of C3PY and C6PY were constructed by re-optimized the geometries at the given dihedral. To simplify our calculation model, the PES was constructed by only altering one of the two rotatable double bonds, while the another double bond was frozen at E-configuration, the step size is set to 30°, and the initial dihedral value is set to -180°. Fig. 6 (a) demonstrates that there is a small energy barrier when the  $T_1$  of C3PY tends to rotate out of the plane. While for C6PY, the  $T_1$  is at high position when it retains at E, E configuration, that is, the  $T_1$  of C6PY has great tendency to rotate out of its original plane. When the dihedral is rotated to -90°, the  $T_1$ - $S_0$  energy difference for C3PY is 12.05 kcal/mol, while this value is 6.83 kcal/mol for C6PY. This relatively small energy

difference further proves that the triplet state of C6PY has higher probability to drop to the high vibrational level of ground state at conical intersection (Scheme 3), after which double bond isomerization occurred during IC. This result is in line with their fast isomerization and low photochemical reactivity of C6PY.

However, at this stage, two questions are still not clear: why does the photo-isomer of C6PY, C6NPY, C6SPY cannot go back to their original lowest states under dark condition and why there is no spectral evidence of the isomer of C3PY? Theoretically, after conical intersection, the high vibrational level of  $S_{0n}$  state is achieved, and this state has equal probability to reach the different isomer through double bond rotation during IC, which finally results in isomerization. It is postulated that, the absent observation of C3PY isomer in photolysis experiment could be ascribed to its high photochemical reactivity, that is, photobleaching occurred in both isomers rapidly. As to C6 series, it is deduced that the high vibrational state cannot reach the original geometry because of steric hindrance between six-member ring and pyrrole group. It is needed to note that the double bond rotation, the root of excited energy dissipation, is inherent in both PYOs isomer even the photo-isomerization is not observed in spectra characterization. The rate of double bond rotation, which could be reflected by the  $K_{IC}$ , is a determined parameter for a specific photoreaction.

## 4. Conclusions

Four pyrrole-based enone dyes (PYOs) with different ketone structure were synthesized to investigate the influence of ketone part on their photochemical and photophysical properties. It was established that the ketone part has little effect on their absorption properties but strongly change their photophysical properties, especially fluorescence emission quantum yield. As a result, the initiation performance of PYOs in radical

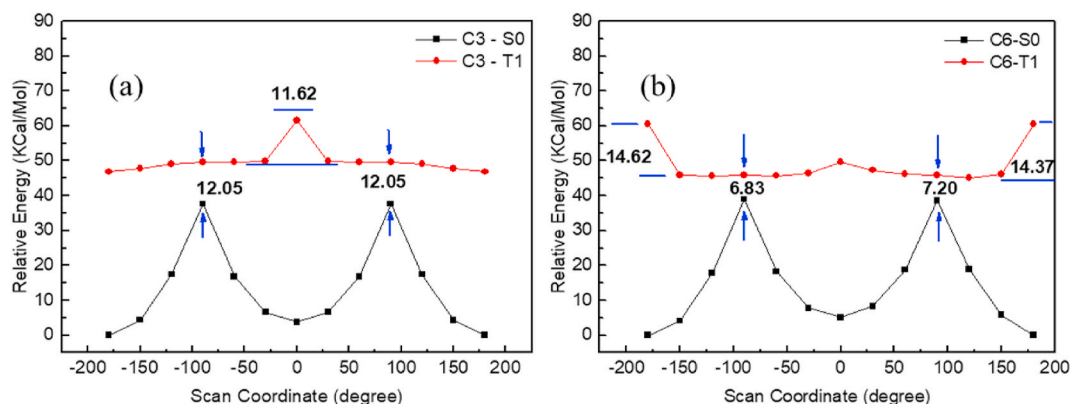


Fig. 6. Potential energy surfaces of  $T_1$  and  $S_0$  along with the dihedral variation as highlighted in Fig. 5 during double bond rotation (a) C3PY (b) C6PY.

photopolymerization varied a lot. Among them, C3PY displayed best performance. According to the photolysis experiment and DFT calculation, it is found C6PY, C6NPY, and C6SPY are more likely to deactivate their excited energy through internal conversion, namely, double bond rotation, which resulted in their low photochemical reactivity. This work indicated that imposing a six-member ring on ketone part is detrimental to the photochemical reactivity of pyrrole-based enone dyes for photoinitiation application, which may provide meaningful information to the other types of enone dyes photoinitiator.

### CRedit authorship contribution statement

**Tanlong Xue:** Conceptualization, Data curation, Formal analysis, Investigation, Methodology, Software, Writing – original draft, Writing – review & editing. **Yang Li:** Data curation, Investigation, Methodology, Synthesis, Data curation, Investigation, Methodology. **Liqun Tang:** Synthesis. **Ruifen Tang:** Investigation. **Jun Nie:** Funding acquisition, Resources, Supervision. **Xiaoqun Zhu:** Resources, Funding acquisition, Supervision, Formal analysis, Writing – review & editing.

### Declaration of competing interest

The authors declare that they have no known competing financial interests or personal relationships that could have appeared to influence the work reported in this paper.

### Acknowledgments

This study was financially supported by the National Key Research and Development Program of China (2017YFB0307800). The authors appreciate the support of the Beijing Laboratory of Biomedical Materials. We also thank the Beijing University of Chemical Technology CHEMCLOUDCOMPUTING Platform for support with calculations.

### Appendix A. Supplementary data

Supplementary data to this article can be found online at <https://doi.org/10.1016/j.dyepig.2021.109372>.

### References

- [1] P FJ. Photoinitiators for polymer synthesis: scope, reactivity, and efficiency. John Wiley & Sons; 2012.
- [2] Yagci Y, Jockusch S, Turro NJ. Photoinitiated polymerization: advances, challenges, and opportunities. *Macromolecules* 2010;43(15):6245–60.
- [3] Shao J, Huang Y, Fan Q. Visible light initiating systems for photopolymerization: status, development and challenges. *Polym Chem* 2014;5(14):4195–210.
- [4] Xiao P, Zhang J, Dumur F, Tehfe MA, Morlet-Savary F, Graff B, Gigmès D, Fouassier JP, Lalevée J. Visible light sensitive photoinitiating systems: recent progress in cationic and radical photopolymerization reactions under soft conditions. *Prog Polym Sci* 2015;41:32–66.
- [5] Shi S, Croutxé-Barghorn C, Allonas X. Photoinitiating systems for cationic photopolymerization: ongoing push toward long wavelengths and low light intensities. *Prog Polym Sci* 2017;65:1–41.
- [6] Dietlin C, Schweizer S, Xiao P, Zhang J, Morlet-Savary F, Graff B, Fouassier J-P, Lalevée J. Photopolymerization upon LEDs: new photoinitiating systems and strategies. *Polym Chem* 2015;6(21):3895–912.
- [7] Han W, Shi Y, Xue T, Wang T. Synthesis and electrochemical, linear and third-order nonlinear optical properties of ferrocene-based D- $\pi$ -A dyes as novel photoredox catalysts in photopolymerization under visible LED irradiations. *Dyes Pigments* 2019;166:140–8.
- [8] Jia X, Han W, Xue T, Zhao D, Li X, Nie J, Wang T. Diphenyl sulfone-based A- $\pi$ -D- $\pi$ -A dyes as efficient initiators for one-photon and two-photon initiated polymerization. *Polym Chem* 2019;10(17):2152–61.
- [9] Ay E, Raad Z, Dautel O, Dumur F, Wantz G, Gigmès D, Fouassier J-P, Lalevée J. Oligomeric photocatalysts in photoredox catalysis: toward high performance and low migration polymerization photoinitiating systems. *Macromolecules* 2016;49(6):2124–34.
- [10] Sun X, Jin M, Wu X, Pan H, Wan D, Pu H. Bis-substituted thiophene-containing oxime sulfonates photoacid generators for cationic polymerization under UV-visible LED irradiation. *J Polym Sci Polym Chem* 2018;56(7):776–82.
- [11] Jin M, Zhou R, Yu M, Pan H, Wan D. D- $\pi$ -a-type oxime sulfonate photoacid generators for cationic polymerization under UV-visible LED irradiation. *J Polym Sci Polym Chem* 2018;56(11):1146–54.
- [12] Wu XY, Malval JP, Wan DC, Jin M. D- $\pi$ -A-type aryl dialkylsulfonium salts as one-component versatile photoinitiators under UV/visible LEDs irradiation. *Dyes Pigments* 2016;132:128–35.
- [13] Wu X, Jin M, Xie J, Malval JP, Wan D. One/two-photon cationic polymerization in visible and near infrared ranges using two-branched sulfonium salts as efficient photoacid generators. *Dyes Pigments* 2016;133:363–71.
- [14] Li Z, Zou X, Zhu G, Liu X, Liu R. Coumarin-based oxime esters: photobleachable and versatile unimolecular initiators for acrylate and thiol-based click photopolymerization under visible light-emitting diode light irradiation. *ACS Appl Mater Interfaces* 2018;10(18):16113–23.
- [15] Jia X, Zhao D, You J, Hao T, Li X, Nie J, Wang T. Acetylene bridged D-( $\pi$ -A)<sub>2</sub> type dyes containing benzophenone moieties: photophysical properties, and the potential application as photoinitiators. *Dyes Pigments* 2021;184:108583.
- [16] Zhou R, Malval J-P, Jin M, Spangenberg A, Pan H, Wan D, Morlet-Savary F, Knopf S. A two-photon active chevron-shaped type I photoinitiator designed for 3D stereolithography. *Chem Commun* 2019;55(44):6233–6.
- [17] Yu J, Gao Y, Jiang S, Sun F. Naphthalimide aryl sulfide derivative norrish type I photoinitiators with excellent stability to sunlight under near-UV LED. *Macromolecules* 2019;52(4):1707–17.
- [18] Nazir R, Danilevicius P, Ciuciu AI, Chatzinikolaïdou M, Gray D, Flamigni L, Farsari M, Gryko DT.  $\pi$ -Expanded ketocoumarins as efficient, biocompatible initiators for two-photon-induced polymerization. *Chem Mater* 2014;26(10):3175–84.
- [19] Li Z, Pucher N, Cicha K, Torgersen J, Ligon SC, Ajami A, Husinsky W, Rosspeintner A, Vauthey E, Naumov S, Scherzer T, Stampfl J, Liska R. A straightforward synthesis and structure–activity relationship of highly efficient initiators for two-photon polymerization. *Macromolecules* 2013;46(2):352–61.
- [20] Wu J, Shi M, Zhao Y, Wu F. Two-photon absorption property and photopolymerization sensitizing efficiency of asymmetrical benzylidene cyclopentanone dyes. *Dyes Pigments* 2008;76(3):690–5.
- [21] Wu J, Zhao Y, Li X, Shi M, Wu F, Fang X. Multibranch benzylidene cyclopentanone dyes with large two-photon absorption cross-sections. *New J Chem* 2006;30(7):1098.
- [22] Huang X, Wang X, Zhao Y. Study on a series of water-soluble photoinitiators for fabrication of 3D hydrogels by two-photon polymerization. *Dyes Pigments* 2017;141:413–9.
- [23] Huang X, Zhang Y, Shi M, Zhang Y, Zhao Y. Study on a polymerizable visible light initiator for fabrication of biosafety materials. *Polym Chem* 2019;10(18):2273–81.
- [24] Fu H, Qiu Y, You J, Hao T, Fan B, Nie J, Wang T. Photopolymerization of acrylate resin and ceramic suspensions with benzylidene ketones under blue/green LED. *Polymer* 2019;184:121841.
- [25] Hu T, Fu H, Xiong J, Wang T. Benzylidene piperidones as photosensitizers for visible light photopolymerization. *J Photochem Photobiol Chem* 2021;405:112968.
- [26] Li J, Hao Y, Zhong M, Tang L, Nie J, Zhu X. Synthesis of furan derivative as LED light photoinitiator: one-pot, low usage, photobleaching for light color 3D printing. *Dyes Pigments* 2019;165:467–73.
- [27] Tang L, Nie J, Zhu X. A high performance phenyl-free LED photoinitiator for cationic or hybrid photopolymerization and its application in LED cationic 3D printing. *Polym Chem* 2020;11(16):2855–63.
- [28] Yang F, Zhong M, Zhao X, Li J, Sun F, Nie J, Zhu X. High efficiency photoinitiators with extremely low concentration based on furans derivative. *J Photochem Photobiol Chem* 2021;406:112994.
- [29] Xu Y, Noirbent G, Brunel D, Ding Z, Gigmès D, Graff B, Xiao P, Dumur F, Lalevée J. Allyloxy ketones as efficient photoinitiators with high migration stability in free radical polymerization and 3D printing. *Dyes Pigments* 2021;185:108900.
- [30] Xu Y, Noirbent G, Brunel D, Liu F, Gigmès D, Sun K, Zhang Y, Liu S, Morlet-Savary F, Xiao P, Dumur F, Lalevée J. Ketone derivatives as photoinitiators for both radical and cationic photopolymerizations under visible LED and application in 3D printing. *Eur Polym J* 2020;132:109737.
- [31] Sun K, Xu Y, Dumur F, Morlet-Savary F, Chen H, Dietlin C, Graff B, Lalevée J, Xiao P. In silico rational design by molecular modeling of new ketones as photoinitiators in three-component photoinitiating systems: application in 3D printing. *Polym Chem* 2020;11(12):2230–42.
- [32] Chen H, Noirbent G, Sun K, Brunel D, Gigmès D, Morlet-Savary F, Zhang Y, Liu S, Xiao P, Dumur F, Lalevée J. Photoinitiators derived from natural product scaffolds: monochalcones in three-component photoinitiating systems and their applications in 3D printing. *Polym Chem* 2020;11(28):4647–59.
- [33] Chen H, Noirbent G, Zhang Y, Brunel D, Gigmès D, Morlet-Savary F, Graff B, Xiao P, Dumur F, Lalevée J. Novel D- $\pi$ -A and A- $\pi$ -D- $\pi$ -A three-component photoinitiating systems based on carbazole/triphenylamino based chalcones and application in 3D and 4D printing. *Polym Chem* 2020;11(40):6512–28.
- [34] Xu Y, Noirbent G, Brunel D, Ding Z, Gigmès D, Graff B, Xiao P, Dumur F, Lalevée J. Novel ketone derivative-based photoinitiating systems for free radical polymerization under mild conditions and 3D printing. *Polym Chem* 2020;11(36):5767–77.
- [35] Stansbury JW, Dickens SH. Determination of double bond conversion in dental resins by near infrared spectroscopy. *Dent Mater* 2001;17(1):71–9.
- [36] Li J, Zhang X, Ali S, Akram MY, Nie J, Zhu X. The effect of polyethylene glycol diacrylate complexation on type II photoinitiator and promotion for visible light initiation system. *J Photochem Photobiol Chem* 2019;384:112037.

- [37] Xue T, Tang L, Tang R, Li Y, Nie J, Zhu X. Color evolution of a pyrrole-based enone dye in radical photopolymerization formulations. *Dyes Pigments* 2021;188: 109212.
- [38] Crivello JV. The discovery and development of onium salt cationic photoinitiators. *J Polym Sci Polym Chem* 1999;37(23):4241–54.
- [39] Mau A, Le TH, Dietlin C, Bui T-T, Graff B, Dumur F, Goubard F, Lalevee J. Donor–acceptor–donor structured thioxanthone derivatives as visible photoinitiators. *Polym Chem* 2020;11(45):7221–34.
- [40] Han W-G, Lovell T, Liu T, Noodleman L. Density functional studies of the ground- and excited-state potential-energy curves of stilbene cis–trans isomerization. *ChemPhysChem* 2002;3(2):167–78.
- [41] Al Mousawi A, Dumur F, Garra P, Toufaily J, Hamieh T, Graff B, Gignes D, Fouassier JP, Lalevee J. Carbazole scaffold based photoinitiator/photoredox catalysts: toward new high performance photoinitiating systems and application in LED projector 3D printing resins. *Macromolecules* 2017;50(7):2747–58.
- [42] Bonačić-Koutecký V, Michl J. Photochemical syn-anti isomerization of a Schiff base: a two-dimensional description of a conical intersection in formalimine. *Theor Chim Acta* 1985;68(1):45–55.
- [43] Reguero M, Olivucci M, Bernardi F, Robb MA. Excited-state potential surface crossings in acrolein: a model for understanding the photochemistry and photophysics of  $\alpha,\beta$ -enones. *J Am Chem Soc* 1994;116(5):2103–14.
- [44] Gaussian 09, Revision D.01, Frisch MJ, Trucks GW, Schlegel HB, Scuseria GE, Robb MA, Cheeseman JR, Scalmani G, Barone V, Mennucci B, Petersson GA, Nakatsuji H, Caricato M, Li X, Hratchian HP, Izmaylov AF, Bloino J, Zheng G, Sonnenberg JL, Hada M, Ehara M, Toyota K, Fukuda R, Hasegawa J, Ishida M, Nakajima T, Honda Y, Kitao O, Nakai H, Vreven T, Montgomery Jr JA, Peralta JE, Ogliaro F, Bearpark M, Heyd JJ, Brothers E, Kudin KN, Staroverov VN, Keith T, Kobayashi R, Normand J, Raghavachari K, Rendell A, Burant JC, Iyengar SS, Tomasi J, Cossi M, Rega N, Millam JM, Klene M, Knox JE, Cross JB, Bakken V, Adamo C, Jaramillo J, Gomperts R, Stratmann RE, Yazyev O, Austin AJ, Cammi R, Pomelli C, Ochterski JW, Martin RL, Morokuma K, Zakrzewski VG, Voth GA, Salvador P, Dannenberg JJ, Dapprich S, Daniels AD, Farkas O, Foresman JB, Ortiz JV, Cioslowski J, Fox DJ. Wallingford CT: Gaussian, Inc.; 2013.